Current oscillations in vanadium dioxide: Evidence for electrically triggered percolation avalanches

Tom Driscoll*
Center for Metamaterials and Integrated Plasmonics, Pratt School of Engineering, Duke University, Durham, North Carolina, 27708, USA and Physics Department, University of California, San Diego, La Jolla, California 92093, USA

Jack Quinn, Massimiliano Di Ventra, and Dimitri N. Basov
Physics Department, University of California, San Diego, La Jolla, California 92093, USA

Giwan Seo
School of Advanced Device Technology, University of Science and Technology (UST), Daejon 305-350, Korea

Yong-Wook Lee
School of Electrical Engineering, Pukyong National University, Busan 608-737, South Korea

Hyun-Tak Kim
School of Advanced Device Technology, University of Science and Technology (UST), Daejon 305-350, Korea and Creative Research Center of Metal-Insulator Transition, ETRI, Daejon 305-700, South Korea

David R. Smith
Center for Metamaterials and Integrated Plasmonics, Pratt School of Engineering, Duke University, Durham, North Carolina 27708, USA
(Received 12 September 2011; revised manuscript received 25 January 2012; published 17 September 2012)

In this work, we experimentally and theoretically explore voltage-controlled oscillations occurring in microbeams of vanadium dioxide. These oscillations are a result of the reversible insulator-to-metal phase transition in vanadium dioxide. By examining the structure of the observed oscillations in detail, we propose a modified percolative-avalanche model which allows for voltage triggering. This model captures the periodicity and waveshape of the oscillations as well as several other key features. Importantly, our modeling shows that while temperature plays a critical role in the vanadium dioxide phase transition, electrically induced heating can not act as the primary instigator of the oscillations in this configuration. This realization leads us to identify the electric field as the most likely candidate for driving the phase transition.

DOI: 10.1103/PhysRevB.86.094203 PACS number(s): 71.30.+h

I. INTRODUCTION

Vanadium dioxide (VO_2) has been a material of prolonged scientific interest due to the plethora of unusual properties associated with the insulator-to-metal phase transition (IMT) occurring just above room temperature.[1] The large conductivity change ratio, combined with an accessible transition temperature and rich correlated-electron physics,[2–4] has made this an attractive compound for many researchers. Much attention has historically revolved around controversy over the driving physics of the phase transition, particularly whether it is a Mott transition[5–7] or Peierls transition.[2,8,9] However, also of interest is the ability of the IMT to happen on ultrafast (100-fs) time scales,[10] and the wide range of stimuli which can trigger it.[11,12] Along these lines, recent interest has also shifted from purely academic to industrial as well: following proposed applications ranging from optical devices[13] and hybrid metamaterials[14–16] to electronics[17–19] and data storage.[20,21] With this rise of potential applications comes opportunities for new avenues of research and development, but also new challenges to satisfy the durability and flexibility that real-world devices demand.[22] Understanding the role of temperature and structural transitions in various VO_2 phenomena is key to pushing towards potential of applications.

In this paper, we take an interest in the recently reported[23,24] phenomenon of self-sustaining oscillations in VO_2 bridges. The widespread prevalence of voltage-controlled oscillators in electronics makes this phenomenon an enticing candidate for devices. It is fairly well accepted that these oscillations represent a triggering of the insulator-to-metal transition, followed by a resetting metal-to-insulator transition (MIT). However, despite headway on controlling such oscillations in VO_2,[24,25] there is still debate over whether the underlying driving mechanism is thermal or electrostatic. In literature, VO_2 is most often thermally triggered, and yet these oscillations appear to respond foremost to applied voltage across the device. The unavoidable presence of joule-heating currents through the two-terminal device during operation, coupled with the observed sensitivity of the oscillations to device temperature,[22,26] make for a contentious situation.

In our investigation, we first experimentally reproduce the oscillations discovered by the authors of Ref. 23. The use of a high-performance oscilloscope in our experiment gives us access to very fine time-resolution data, which is useful in our modeling. The details and data of our experiment are reported in Sec. II. Following this, we develop a model which replicates and explains the observed waveshape in terms of electrically triggered domains. Our model, reported in Sec. III, describes a network of electrically and/or thermally triggered grains. This model is inspired by several previously proposed models.[27,28] While these previous models also predict avalanchelike transitions under the right conditions,[27] our model expands on this framework to track time-dependent effects and allow possibility of a voltage-triggered phase transition. Alongside voltage triggering, we investigate the role of temperature in the oscillations, and importantly, we find while a voltage-driven picture replicates experimental data, thermal heating *alone* is quantitatively and qualitatively unable to explain the structure of the observed oscillations. Nevertheless, device temperature does affect oscillations, and thermal cofactors to the voltage triggering are needed to reproduce aspects of the data. In Sec. IV, we discuss how the percolative transition of VO_2 affects the shape of the MIT, and what this means regarding effective medium within the phase-coexistence region. In Sec. V, we conclude the paper with an overview of our results, and an outlook on possible directions for VO_2 research and application.

II. VOLTAGE-CONTROLLED OSCILLATIONS.

Our investigation begins with replicating VO_2 oscillations using the procedure reported by Kim *et al.*[23,25] A device consisting of a 10 μm × 10 μm VO_2 bridge between two large (≈400 μm) metal (Ni:Au) electrodes (Fig. 1 inset) is hooked in series with a limiting resistor ($R_{\text{ext}} = 15$ kΩ) and voltage source (V_{app}). This setup is shown schematically in Fig. 1. The VO_2 is 100 nm thick, and is prepared via sol-gel deposition in the [1 0 0] orientation. The grains in this preparation are typically found to be 50–100 nm. Although we do not intentionally add external capacitance, the presence of such C_{ext} in instruments and cables is unavoidable and should be included in the effective circuit. The applied voltage V_{app} is a transient square pulse (between 1 μs to 1 ms) from an Agilent function generator (model 33120 A) riding on top of a constant bias voltage ($V_{\text{bias}} = 12$ V). This is shown as the black trace in Fig. 2, giving a peak applied voltage of 22 V. The voltage across the device (V_D, as shown by the blue trace in Fig. 2) is monitored with a LeCroy (model wavepro 7-zi) oscilloscope, which allows for high-time-resolution (40 GS/s) sampling resolution even over millisecond-long pulses.

In this configuration, the VO_2 device functions essentially as a capacitor with a small-signal capacitance $C_D \approxeq 40_p F$ and variable internal shunt resistance R_D. The capacitance C_D is primarily fixed by device geometry, and includes the large electrodes at either side of the VO_2 bridge. Variations of the dielectric constant of VO_2 throughout the phase transition (such as have been shown in the context of memory capacitance[15,29]

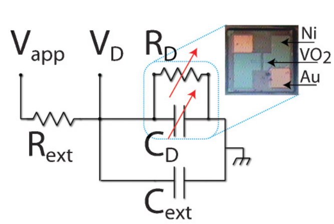

FIG. 1. (Color online) Schematic of the circuit diagram used to reproduce oscillations, depicting the VO_2 device as a variable resistance and capacitance. Inset shows optical photograph of a sample device. The Al_2O_3 substrate is 330 μm thick, and is mounted on a glass cover slip. All experiments are performed at room temperature.

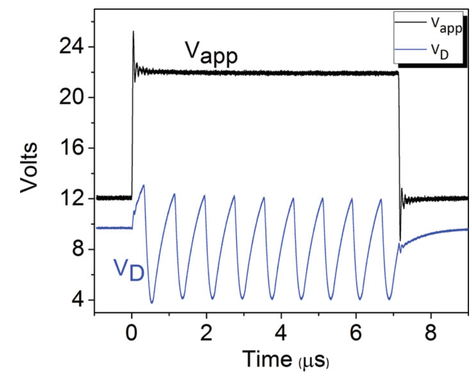

FIG. 2. (Color online) Applied voltage and voltage across the device as a function of time.

and VO_2 hybrid metamaterials[14]) may have small effects, and we discuss this later in Sec. IV B. The prepulse steady-state starting voltage is $V_D = V_{\text{bias}} R_D/(R_D + R_{\text{ext}})$. At the start of the pulse ($t = 0$), V_D increases, following a canonical resistance-capacitance (RC) charging curve. Once V_D surpasses a threshold voltage (which we will call $V_{D:\text{IMT}}$), it transitions sharply from increasing V_D to decreasing. We assign this change to an IMT event occurring in the VO_2, which effectively lowers the internal shunt resistance R_D of the capacitor. With lower internal resistance, the capacitor undergoes rapid discharge, expending its stored energy through the internal resistance R_D, and V_D plummets. This discharge continues until V_D reaches a lower threshold voltage ($V_{D:\text{MIT}}$ at which a second event, which we similarly assign to a MIT restores the high internal device resistance. The process reverses and this sequence of events repeats, alternating charging and discharging between IMT and MIT events with a fairly stable periodicity.[25]

III. GRAIN-SCALE MODEL OF OSCILLATIONS

Our hope is that by developing a model for these observed oscillations, we may gain insight into the driving mechanism behind them. We start with a two-dimensional (2D) network of square VO_2 grains of differing sizes. The resistivity of each grain is dependent on its state (metal or insulator),[30,31] and total resistance is given by the product of grain size and resistivity. The granularity of polycrystalline VO_2 is well documented,[32,33] although the size of grains may vary considerably from one VO_2 preparation to another. There is also evidence to suggest the percolation length scales for the IMT may not always coincide with the crystal granularity.[34–36] A cartoon illustrating our model arrangement is shown in Fig. 3. The network consists of $N_i \times N_j$ grains, and in our model we restrict our investigation to a 50 × 50 network array to keep computation time manageable.

This grain network is placed in an external circuit containing resistance R_{ext} and capacitance C_{ext}, and driven by V_{app}, as shown in Fig. 1. The voltage change across the device is given by the charge conservation circuit equation

$$\frac{d}{dt} V_D(t) = \frac{d}{dt}\left(\frac{Q(t)}{C(t)}\right), \tag{1}$$

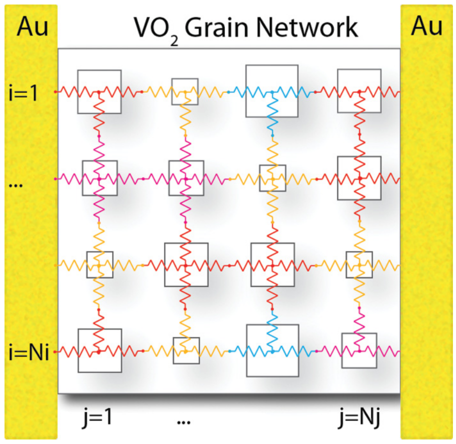

FIG. 3. (Color online) Cartoon of the grains resistor network. Left and right sides are the beginning of the gold electrodes. In the cartoon, the size of the squares represents a distribution of grain sizes, and resistor colors serve to highlight the corresponding different resistance.

which becomes

$$\dot{V}_D(t) = \frac{1}{(C_D + C_{\text{ext}})}\left(\frac{V_{\text{app}} - V_D}{R_{\text{ext}}} - \frac{V_D}{R_D} - \dot{C_D} V_D\right). \tag{2}$$

The circuit differential equation [Eq. (2)] is solved via Runge-Kutta time stepping. At each time step, we solve for the internal state of the grain network. This includes solving a Kirchoff network problem[37] for the voltage across each grain and the Thevenin effective circuit resistance R_D. The other VO_2 effective circuit parameter C_D is found by a differential capacitance equation [Eq. (3)], which can be evaluated via a self-consistent Bruggeman effective medium formulation [Eqs. (4) and (5)]

$$C_D(t) = C_0 + \eta \frac{\epsilon_D}{\epsilon_0}, \tag{3}$$

$$0 = f \frac{\epsilon_m - \epsilon_D}{\epsilon_m + 2\epsilon_D} - (f - 1)\frac{\epsilon_i - \epsilon_D}{\epsilon_i + 2\epsilon_D}, \tag{4}$$

$$f = \frac{\sum^{ij} X^{ij}}{N_i N_j}. \tag{5}$$

Superscripts i and j are row and column indices for the grains (running to N_i and N_j total). The binary matrix $X^{ij} = 1$ if the grain i,j is metal and 0 if insulator. η is a capacitive fractional-fields factor (the proportion of the device capacitance which involves the VO_2 dielectric), which is found via finite element simulation using the COMSOL commercial code package. C_0 is a geometrical capacitance which is determined empirically, fitting 1/RC to the capacitive charging curve. External circuit parameters such as R_{ext} and V_{app} are taken directly from experimental values. The extrema values for R_D (metal) and R_D (insulator) are taken from temperature data.

A. Thermal triggering

The temperature-driven IMT-MIT has been investigated in great detail, and we ground our model using experimental data giving resistance as a function of temperature $R(T)$ through the phase transition. These data are shown in Fig. 4(a), and display the characteristic sharp change in resistivity around 345 K. Then, in a procedure similar to previous works,[6,27] we assume each grain will undergo an IMT in response a "high-threshold" temperature T^{ij}_{IMT}, and a MIT at a low-threshold T^{ij}_{MIT}:

$$R^{ij} = R_{\text{met}} \quad \text{if} \quad \left(T^{ij} > T^{ij}_{\text{IMT}}\right) \tag{6}$$

$$= R_{\text{ins}} \quad \text{if} \quad \left(T^{ij} < T^{ij}_{\text{MIT}}\right). \tag{7}$$

We assign a stochastic distribution to the values of T^{ij}_{IMT} and T^{ij}_{MIT} throughout the network, following the Gaussian form

$$P\left(T^{ij}_{\text{IMT}}\right) = e^{-\frac{(T^{ij}_{\text{IMT}} - T_{0_{\text{IMT}}})}{2\sigma^2_{\text{IMT}}}}, \tag{8}$$

$$P\left(T^{ij}_{\text{MIT}}\right) = e^{-\frac{(T^{ij}_{\text{MIT}} - T_{0_{\text{MIT}}})}{2\sigma^2_{\text{MIT}}}}. \tag{9}$$

The values of T_0 and σ^2 are fit to the experimental $R(T)$ data shown in Fig. 4(a). From this, we find a variance of $T_{0_{\text{IMT}}} = 340$ K and $\sigma^2_{\text{IMT}} = 0.1 * T_{0_{\text{IMT}}}$ reproduces the shape of the IMT fairly well. On the MIT transition, we find $T_{0_{\text{MIT}}} = 330$ K with variance the same as the IMT. This fit gives us confidence that we understand the thermal response of VO_2. It is important to note that although we plot average temperature for visual simplicity, the temperature of each grain (T^{ij}) is accounted separately. Thus, our model accounts for any local fluctuations of temperature that may happen.

Using this temperature-only-triggered model, we attempt to reproduce the oscillations shown in Fig. 2. Our model tracks the power dissipated in each grain and employs a finite-element method to solve for the grain and substrate temperatures as a function of time. Material thermal parameters are taken from literature, and the enthalpy of phase transition for VO_2 is included. Neumann and Dirichlet boundaries are enforced above the VO_2 and at the back of the substrate, respectively. Heat conduction through the electrodes is included as a Neumann boundary at the edges of the VO_2. Figure 4(b) replots our experimental V_D oscillations in blue and the model results in green. The result is striking: although we can track V_D for a short while, we do not observe any oscillatory phenomena.

Generalizing the behavior that prohibits oscillations, thermal-initiated IMTs exhibit a latched-on behavior rather than the self-stabilizing oscillatory nature seen in Fig. 2. This is apparent in the average VO_2 grain temperature plot (red) of Fig. 4(b). Note that although individual different grains may attain different temperatures over the course of oscillations, such gradients equalize quickly within the network. Average temperature remains a fairly accurate and easily visualized metric of the VO_2 oscillation thermodynamics. As the thermally triggered IMT occurs, VO_2 temperature skyrockets even while V_D discharges. This means that for a thermally initiated transition, the onset of the sharp heating associated with discharge begins already above $T_{0_{\text{IMT}}}$, and reaches very high temperatures (>380 K here). Repeated cycling to these high temperatures would likely destroy the device quickly, which is not observed experimentally. Once the temperature of the discharged device has surpassed $T_{0_{\text{IMT}}}$, heating rate remains high, and the device does not cool below $T_{0_{\text{MIT}}}$. Power dissipation and temperature both settle towards steady state with the device firmly in the metallic state. The causes of this process will become more apparent as we discuss thermal dynamics in Sec. III D.

B. Electrical triggering

With the failure of a temperature-*only* triggering model to produce oscillations, and following insights from previous work on voltage-induced effects in VO_2,[23,27,38,39] we now introduce an electric-field-driven transition. To do this, we also assign a *voltage drop* at which each grain undergoes phase transition $V^{ij}_{\rm IMT}$ and $V^{ij}_{\rm MIT}$. We again use random values from a normal distribution as we did for $T^{ij}_{\rm IMT}$ and $T^{ij}_{\rm MIT}$:

$$P\left(V^{ij}_{\rm IMT}\right) = e^{-\frac{(V^{ij}_{\rm IMT} - V_{0_{\rm IMT}})}{2\sigma^2_{\rm IMT}}}, \tag{10}$$

$$P\left(V^{ij}_{\rm MIT}\right) = e^{-\frac{(V^{ij}_{\rm MIT} - V_{0_{\rm MIT}})}{2\sigma^2_{\rm MIT}}}. \tag{11}$$

We lack direct data to which to fit these distributions [as we did in Fig. 4(a)]. Thus, we retain the same value for the variance found in above, $\sigma_V^2 = 0.1 * V_0$. From an energetics perspective, this makes a great deal of sense: both distributions are surely tied to the same underlying Mott physics. V_0 remains a fitting parameter in our model.

As we have not removed possible thermal triggering, the conditions for grain transition can now be stated as

$$R^{ij} = R_{\rm met} \quad \text{if} \quad \left[\left(V^{ij} > V^{ij}_{\rm IMT}\right) \text{ or } \left(T^{ij} > T_{\rm IMT}\right)\right], \tag{12}$$

$$= R_{\rm ins} \quad \text{if} \quad \left[\left(V^{ij} < V^{ij}_{\rm MIT}\right) \text{ and } \left(T^{ij} < T_{\rm MIT}\right)\right]. \tag{13}$$

This combined triggering criterion reproduces both the waveshape and periodicity of the experimentally observed oscillations quite well. In Fig. 5, we replot the experimental data from Fig. 2 in blue, and numerical results from our model are shown overlaid in green. We also observe that within our model, increasing (decreasing) the amplitude of applied voltage increases (decreases) the frequency of oscillations, as reported in previous experiments. This dependence is plotted in Fig. 5(b).

There is one notable difference between the thermally driven IMT shown in Fig. 4 and the electrically triggered model which reproduces oscillations (Fig. 5). We find in order to fit oscillations, the value of $R_{\rm met}$ is 3 kΩ, an order of magnitude less conductive than the $\approx$100 Ω shown at high temperatures in Fig. 4. This can be seen in the resistance plotted in Fig. 9, which will be discussed in more detail in Sec. IV B. Previous experimental work has shown that the onset of the correlated electron state initiating the phase transition does occur before (and at higher resistances than) the fully metallic state observed at temperatures well above $T_{\rm IMT}$.[2,3,36] It may be that electric-only triggering of the IMT only reaches this initial correlated electron state, but such a conclusion requires additional experimental investigation, especially one that may provide a time-resolved probe of local temperature.[40]

C. Voltage-temperature dependence

Although Sec. III B demonstrated that voltage is the primary trigger, device temperature still plays a role in oscillations. There is a known dependence of oscillation amplitude on device temperature.[26] If we look carefully at the data in Fig. 5, we notice a subtle decay envelope to the amplitude of the $V_{\rm IMT}$ oscillation peaks. We believe this envelope is caused by a thermalization of the device on a multioscillation time scale. To accommodate this, we include a temperature dependence to the IMT transition voltage as

$$V^{ij}_{\rm IMT}(T) \rightarrow [\kappa(T - T_0) + 1]V^{ij}_{\rm IMT}, \tag{14}$$

where $T_0 = 295$ K. κ is a linear temperature coefficient, the fitting of which we discuss below. Without including this voltage-temperature interplay, our model quickly loses sync with the experimental data over the course of several oscillation periods. This thermalization envelope is most clearly observed over a long pulse, and experimental data (solid blue) for a 100-μs pulse are shown in Fig. 6. For clarity in this figure, the bottom half of the oscillations is omitted from view

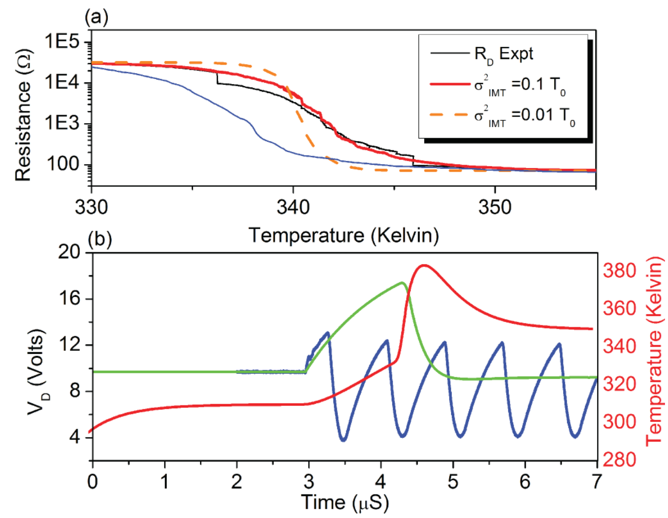

FIG. 4. (Color online) (a) Experimental resistance of our device as a function of temperature $R_D(T)$ (black: heating, blue: cooling). $R_D(T)$ results from our model are overlaid for a best-fit value of variance: $\sigma^2_{\rm IMT} = 0.1 * T_0$ [see Eq. (8)], which replicates the observed temperature-driven IMT fairly well. Also shown is a poor-fit result for $\sigma^2_{\rm IMT} = 0.01 * T_0$, given to show the effect of this parameter. (b) Attempt to replicate oscillations using thermal-only triggering, with values of $P(T^{ij}_{\rm IMT})$ from above. We plot V_D from our model (green) overlaid on experimental V_D (blue). We observe no oscillations, only a single IMT event. We also plot the average VO_2 temperature T_D from our model, illustrating a runaway heating behavior that precludes oscillations.

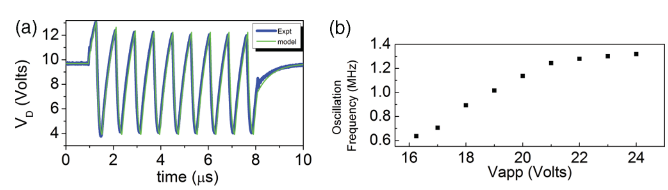

FIG. 5. (Color online) (a) The experimental data from Fig. 2 replotted (blue) with numerical results from our model overlaid (green). This electrical-and-thermal triggering model replicates the experimental data quite well, tracking the oscillation periodicity and producing similar transitions at both $V_{D:\rm IMT}$ and $V_{D:\rm MIT}$. (b) The electrical-triggering model also displays oscillation-frequency dependence on the applied voltage as reported in previous experimental work (Ref. 25).

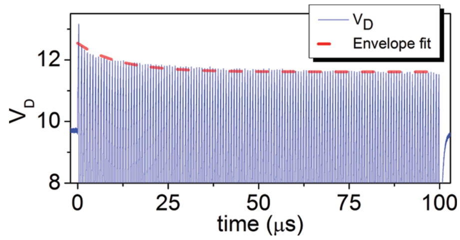

FIG. 6. (Color online) Experimental data (blue) for oscillations over a long 100-μs $V_{\rm app}$ pulse. We observe a clear decay envelope to the amplitude of $V_{\rm IMT}$ in the oscillations. For clarity, the bottom half of the oscillations is omitted as we observe no enveloping here. To show this decay is a thermalization envelope caused by device heating, we also plot the temperature-dependent $V_{\rm IMT}(T)$ from Eq. (14) (red).

(interestingly, we observe no envelope of $V_{\rm MIT}$). Using the data from Fig. 6 combined with our thermal finite element model, we can fit a value for κ. Overlaid on the experimental data (dashed line) is this fit, which gives $\kappa = -8.3 \times 10^{-3}$. This value of κ is used in our oscillation model.

Explanation of this long-time-scale thermalization is straightforward. Although locally the VO_2 film may heat or cool quite quickly in response to current through its volume, the 330-μm-thick sapphire substrate is comparatively massive. The large thermal inertia of the substrate smooths out oscillatory heating away from the film, and when heated only from the top the substrate can require tens of microseconds to reach a steady-state temperature gradient.

D. Temperature dynamics

In Sec. III C, we have discussed the critical interplay between temperature and voltage triggering, showing how a long multioscillation time-scale thermalization envelopes the oscillation amplitude. Previous work has also reported on thermalization time scales in VO_2.[41,42] In this section, we look closer at the temperature evolution on the time scale of the oscillation period.

To begin, in Fig. 7 we plot the average grain temperature (red) during oscillations along with V_D (green), both from our model. Looking at Fig. 7 quantitatively, we notice that the average temperature reached is not sufficient to *trigger* oscillations. Although the peak average temperature during the discharge cycle of the oscillation comes close to reaching $T_{\rm IMT}$, a thermal-driving event would have to occur at or before the peak in V_D. The model results indicate that the device is well below $T_{\rm IMT}$ when $V_{D:\rm IMT}$ is reached. The temperature range in Fig. 7 agrees fairly well with previous numerical work on the subject,[43] and our own investigations using commercial finite element package COMSOL. Compared to COMSOL, our home-grown finite-element code overestimates temperatures reached, perhaps due to difficulty in modeling all of the spatially massive substrate (this is not an issue for commercial packages such as COMSOL). However, commercial codes can not be run from within Runge-Kutta time stepping of Eq. (2), and our code thus critically allows us to calculate temperature dynamics *during* oscillations.

Although a quantitative argument for nonthermal triggering seems compelling, we are acutely aware that precisely solving for temperature can be difficult in such nanoscale systems.

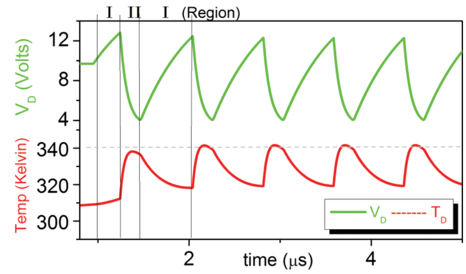

FIG. 7. (Color online) Model results of temperature dynamics during V_D oscillations. The horizontal dashed line at $T_{\rm IMT} = 340$ K shows mean transition temperature, and demonstrates that the average temperature reached during oscillations only comes near to what is needed to drive the IMT transition at the heating peak, after the IMT discharge event. The temperature begins from the steady-state value of 310 K reached under extended $V_{\rm bias}$. We also divide the oscillation into insulating/charging regions (I) and metallic/discharge regions (II). This draws attention to the sharp *increase* in temperature which occurs only *after* the $V_{\rm IMT}$ trigger, qualitatively discrediting a thermal-driving picture for oscillations.

Material properties can differ from published bulk values, and interface effects can dominate transport and heating.[44] As we look closely, though, the power dissipation in the device also appears *qualitatively* unfit to explain the oscillations. A thermally driven transition would have to follow the logical sequence:

(i) The insulating device heats with applied V_D until it reaches $T_{\rm IMT}$, where it undergoes an IMT (becoming metallic).
(ii) The metallic device discharges its stored capacitive energy through the its own volume, cooling as it discharges, until it reaches $T_{\rm MIT}$ where it undergoes MIT (becoming insulating).
(iii) The process repeats.

However, Fig. 7 illustrates that region II, which occurs after $V_{D:\rm IMT}$, is a region of *maximum* power dissipation: a region of heating not cooling. A simple Ohms-law argument explains the following: Just before and just after the IMT, V_D is approximately $V_{D:\rm IMT}$. However, the resistance R_D has changed by a factor of 10, and thus the power dissipated ($P = V_{D:\rm IMT}^2 R_D$) is substantially greater during region II than during region I. Thus, we come to the conclusion that a purely thermal explanation for the oscillations is *qualitatively* as well as quantitatively mismatched to experimental data.

Summarizing Sec. III, we have identified voltage as a key player in triggering observed oscillations on the grounds of several thermal arguments. One interesting question then is whether electrostatic voltage may also trigger the IMT in a current-free [i.e., field-effect transistor (FET)] configuration. The joule heating present in our two-terminal device complicates matters, in light of the voltage/temperature interplay identified in Sec. III C. Previous work has suggested such electrostatic switching can exist,[6,45,46] although these early results await further confirmation. Exploring the phase space defined by the interplay of temperature, electrostatic field, and current in these VO_2 oscillations may reveal information about the correlated electron dynamics and energy scales associated with the Mott transition.

IV. PERCOLATION

In this section, we go into further detail on the mechanisms of the IMT and MIT transitions. Polycrystalline VO_2 is known to exhibit percolative behavior during phase transition,[2,27,35,47] and this has interesting effects on a voltage-triggered transition. Using the model from Sec. III, which accurately predicts the observed electrical oscillations, we attempt to gain insight on several of the internal processes during oscillatory events.

A. Percolative-avalanche-driven oscillations

In several previous works,[27,28] avalanchelike MIT and IMT transitions have been observed under the right conditions. The immediacy of the observed change from charging to discharging in our oscillations leads us to suspect similar avalanche behavior in our electrically driven device. By examining the details of our model, we see that the voltage drop across any grain in the network (see Fig. 3) is proportional to the resistance of the grain. During the charging cycle of the waveform, voltage across the entire device (V_D) increases, and V^{ij} across each grain does as well. This charging continues until one "unlucky" grain hits its V^{ij}_{IMT} first. Because the grains receive a stochastic distribution for V^{ij}_{IMT} [see Eq. (10)], this can be a random grain anywhere in the network. In experiments, it is seen that the phase transition is often seeded at particular places such as defects or boundaries.

The unlucky grain that first hits its IMT trigger condition undergoes an IMT. Once this grain becomes metallic, it supports a lower voltage drop ($R_{\mathrm{ins}}/R_{\mathrm{met}} \approx 20$), which shifts much of its voltage burden to neighboring grains. The neighboring grains in turn become increasingly likely to undergo their own IMT events. The IMT spreads across the entire sample in an avalanchelike manner. This process is depicted in Fig. 8(a) for a network of 50×50 grains. The upper sequence of black and white frames shows whether each grain is insulating (white) or metallic (black). The lower color frames depict the voltage drop across each grain. The neighbor-neighbor grain interaction, mediated by voltage drop, is quite evident.

As is common in percolative systems, the Thevenin resistance R_D of the network is quite sensitive to the spatial distribution of triggered grains. The device resistivity R_D is shown above each frame in the sequence of Fig. 8, and we see the largest drop occurs in frames 6 and 7, where the percolation path is completed from left to right. Once a conducting path forms, R_D plummets and V_D begins to drop as the device discharges.

During discharge, there comes a point where V_D drops far enough that a similar process happens in reverse. This MIT is depicted in Fig. 8(b). However, the MIT process is *not* exactly the reverse of the IMT. The equations governing resistors in parallel tend to "favor" low resistances in the following manner: Decreasing the value of one resistor (in a parallel network) lowers the Thevenin resistance significantly, but raising the value of a single resistor has only a little effect on the Thevenin resistance. For this reason, the avalanchelike behavior observed in Fig. 8(a) is not seen in Fig. 8(b). Instead, the process much more closely resembles random percolation, with only moderate neighbor-neighbor interaction. This difference in the mechanisms between IMT and MIT may explain the difference in sharpness of the transitions at $V_{D_{\mathrm{IMT}}}$ and $V_{D_{\mathrm{MIT}}}$ observed in experiments.[25]

B. Effective medium effects

The percolative nature of the VO_2 phase transition allows for an inhomogeneous intermediate state where both metallic and insulating VO_2 coexist. The dielectric constants of metal and insulating phase VO_2 are distinct, and when both phases can be present in a composite, it leads to interesting properties. The average response of the inhomogeneous sample is described by an effective medium, and can have radically different values than either. This leads to quite interesting and novel effects. For example, the inhomogeneity[2,36] of polycrystalline VO_2 mid-transition is responsible for observed memristance[20]

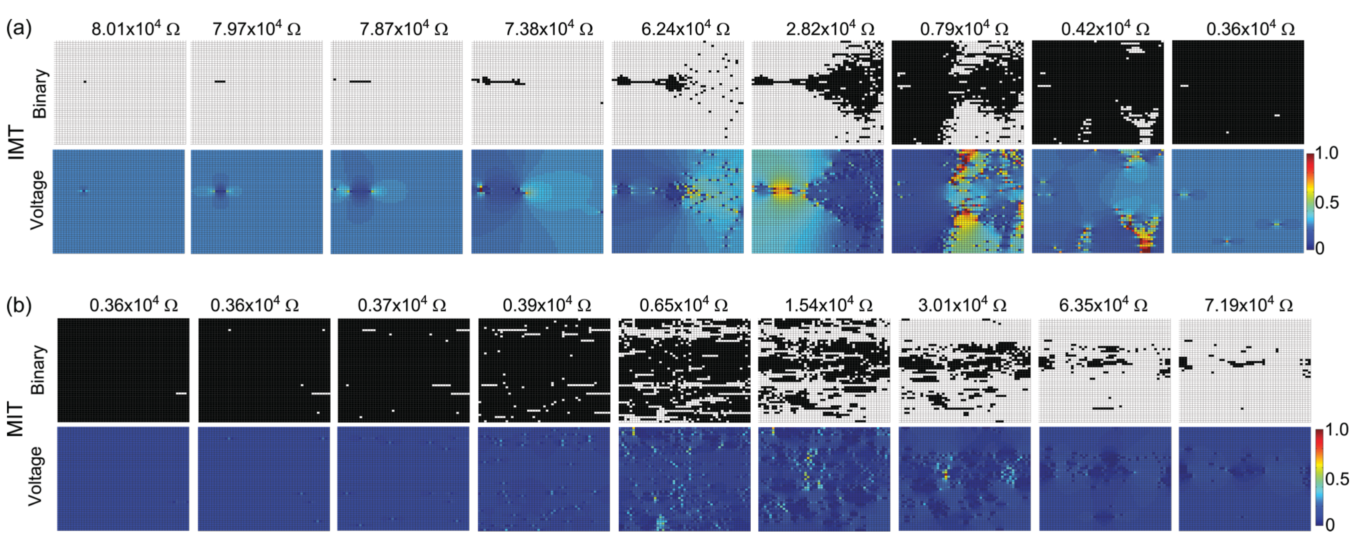

FIG. 8. (Color online) Step-by-step depiction of the avalanchelike transition for a 50×50 grain network. The time of each frame increases from left to right. (a) Shows the IMT transition occurring at $V_{D:\mathrm{IMT}}$, giving a bicolor plot (top) indicating whether each grain is metallic or insulating and the voltage (bottom) across each grain in the network. (b) Shows the same plots for the MIT transition occurring at $V_{D:\mathrm{MIT}}$.

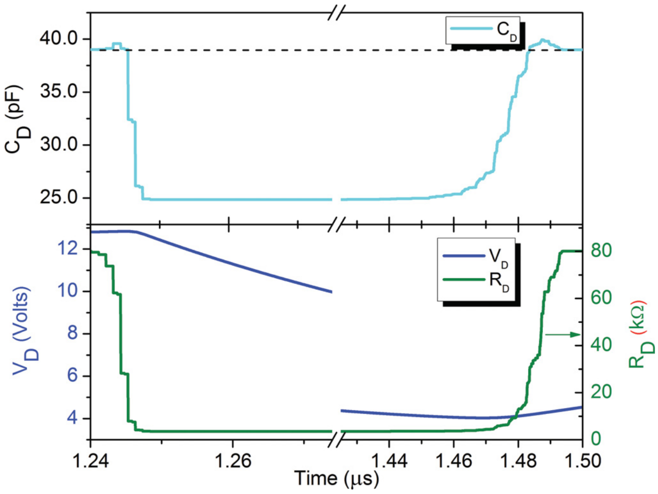

FIG. 9. (Color online) Model values for C_D plotted with V_D and R_D over one oscillation period. Effective medium within the VO_2 [see Eq. (3)] causes a brief spike in C_D immediately near the IMT and MIT transitions. As seen, this spike effect is quite small compared to the overall change of both C_D and R_D, and exists only for a very brief fraction of the oscillation period. The jagged shape of the model curves for R_D and C_D reveal the small jumps typical of percolation discussed in Sec. IV A.

and memory capacitance.[15,29] The same memory capacitance as reported in Ref. 15 has previously been attributed as playing a key role in voltage-controlled oscillations in VO_2.[25] This is a question we are situated to investigate in more depth using our model. To look closely at the effects of capacitance on the oscillations, we focus attention on a single IMT transition event. In Fig. 9, we plot $C_D(t)$ [as calculated from Eqs. (3)–(5)] along with the familiar V_D and R_D.

Looking at Fig. 9, as VO_2 transitions from insulating to metallic at the IMT, R_D drops monotonically to its metallic-state value. The capacitance C_D, however, briefly increases before also decreasing to its metallic-state value. This increase is due to the coexistence of metallic and insulating grains, and is predicted by effective medium [Eq. (5)]. However, as Fig. 9 shows, the increase in C_D is a small effect, and is contained to a short time span near the start of the IMT. This leads us to believe the effective medium behavior of C_D has only a minor influence on the shape of the oscillations, and is not a primary driver. We observe the same increase in C_D at the MIT transition edge, but it also is too small and short lived an effect to bear responsibility for the oscillations.

V. SUMMARY

In this work, we have discussed the thermal and electrical driving mechanisms behind observed oscillations occurring in VO_2 films. In addition to experimentally confirming the oscillations reported by Lee *et al.*,[23] we have compiled a numerical model which is able to replicate and explain these oscillations in terms of a voltage-triggered insulator-to-metal phase transition. Temperature is known to trigger the IMT in VO_2, and temperature plays some role in the shape of the oscillations. However, we find that temperature-only triggering can not explain oscillations. This may carry positive implications for applications, as repeated thermal cycling typically appreciably shortens device lifetime. It also connects to work reporting oscillations in other phase-transition materials.[48]

One question that remains unaddressed is the role, if any, of the structural phase transition in an electric-field-triggered transition. The temperature-driven IMT in VO_2 exhibits a structural transition that happens concurrent with the electronic reconfiguration. However, there is evidence[2,6,35,49–54] to suggest that the electronic and structural transitions are not necessarily linked, but merely overlaid. This structural electronic decoupling suggests the electronic correlations in VO_2 play an important role in the IMT phase transition.

Studies which probe the crystal structure simultaneous with these oscillations have not yet been reported, likely because the time and length scales associated with the VO_2 oscillator devices greatly complicate experiments such as x-ray diffraction. However, as mentioned in the Introduction (Sec. I), the question as to whether or not the structural transition occurs has great implications about the longevity of these devices. In many applications, devices could easily be expected to perform 10^{12} to 10^{14} oscillation events over their lifetime, a likely impossibility if crystallographic changes are occurring. An evident goal for the near future is to experimentally investigate the existence of structural transition in oscillations.

ACKNOWLEDGMENTS

T.D. acknowledges support from an IC postdoctoral fellowship. M.D. acknowledges partial support from NSF. This research is supported by AFOSR and ETRI.

*tom.driscoll@duke.edu

[1] F. J. Morin, Phys. Rev. Lett. **3**, 34 (1959).

[2] Mumtaz M. Qazilbash, Markus Brehm, Byung-Gyu Chae, P.-C. Ho, Gregory O. Andreev, Bong-Jun Kim, Sun Jin Yun, A. V. Balatsky, M. B. Maple, Fritz Keilmann, Hyun-Tak Kim, and Dimitri N. Basov, Science **318**, 1750 (2007).

[3] Mumtaz M. Qazilbash, A. A. Schafgans, K. S. Burch, S. J. Yun, B. G. Chae, B. J. Kim, Hyun-Tak Kim, and D. N. Basov, Phys. Rev. B **77**, 115121 (2008).

[4] M. Liu, B. Pardo, M. M. Qazilbash, S. J. Yun, B. G. Chae, B. J. Kim, D. N. Basov, and R. D. Averitt, in *Lasers and Electro-Optics, 2009 and 2009 Conference on Quantum Electronics and Laser Science Conference. CLEO/QELS 2009* (IEEE, Piscataway, NJ, 2009) Vol. 4, pp. 1–2.

[5] A. Zylbersztejn and N. F. Mott, Phys. Rev. B **11**, 4383 (1975).

[6] Hyun-Tak Kim, B. G. Chae, D. H. Youn, S. L. Maeng, G. Kim, K. Y. Kang, and Y. S. Lim, New J. Phys. **6**, 52 (2004).

[7] T. M. Rice, H. Launois, and J. P. Pouget, Phys. Rev. Lett. **73**, 3042 (1994).

[8] Renata M. Wentzcovitch, Werner W. Schulz, and Philip B. Allen, Phys. Rev. Lett. **72**, 3389 (1994).

[9] Andrea Cavalleri, Th. Dekorsy, H. Chong, J. Kieffer, and R. Schoenlein, Phys. Rev. B **70**, 161102 (2004).
[10] Andrea Cavalleri, Cs. Tóth, C. W. Siders, J. A. Squier, F. Ráksi, P. Forget, and J. C. Kieffer, Phys. Rev. Lett. **87**, 237401 (2001).
[11] Matteo Rini, Andrea Cavalleri, Robert W. Schoenlein, René López, Leonard C. Feldman, Richard F. Haglund, Lynn A. Boatner, and Tony E. Haynes, Opt. Lett. **30**, 1 (2005).
[12] S. Lysenko, A. J. Rua, V. Vikhnin, J. Jimenez, F. Fernandez, and H. Liu, Appl. Surf. Sci. **252**, 5512 (2006).
[13] ReneÌ Lopez, L. A. Boatner, T. E. Haynes, R. F. Haglund, and L. C. Feldman, Appl. Phys. Lett. **85**, 1410 (2004).
[14] Tom Driscoll, S. Palit, Mumtaz M. Qazilbash, Markus Brehm, Fritz Keilmann, Byung-Gyu Chae, Sun-Jin Yun, Hyun-Tak Kim, Nan Marie Jokerst, David R. Smith, and Dimitri N. Basov, Appl. Phys. Lett. **93**, 024101 (2008).
[15] Tom Driscoll, Hyun-Tak Kim, Byung-Gyu Chae, Bong-Jun Kim, Yong-Wook Lee, Nan Marie Jokerst, S. Palit, David R. Smith, Massimiliano Di Ventra, and Dimitri N. Basov, Science **325**, 1518 (2009).
[16] Matthew J. Dicken, Koray Aydin, Imogen M. Pryce, Luke A. Sweatlock, M. Boyd, Sameer Walavalkar, James Ma, and Harry A. Atwater, Opt. Express **17**, 295 (2009).
[17] B. J. Kim, Y. W. Lee, B. G. Chae, S. J. Yun, S. Y. Oh, Y. S. Lim, and Hyun-Tak Kim, Appl. Phys. Lett. **90**, 023515 (2007).
[18] Tom Driscoll, J. Quinn, S. Klein, Hyun-Tak Kim, B. J. Kim, Yuriy V. Pershin, Massimiliano Di Ventra, and D. N. Basov, Appl. Phys. Lett. **97**, 093502 (2010).
[19] Zheng Yang, Changhyun Ko, and Shriram Ramanathan, Annu. Rev. Mater. Res. **41**, 337 (2010).
[20] Tom Driscoll, Hyun-Tak Kim, B. G. Chae, Massimiliano Di Ventra, and D. N. Basov, Appl. Phys. Lett. **95**, 043503 (2009).
[21] Y. V. Pershin, Adv. Phys. **60**, 145 (2011).
[22] Aurelian Crunteanu, Julien Givernaud, Jonathan Leroy, David Mardivirin, Corinne Champeaux, Jean-Christophe Orlianges, Alain Catherinot, and Pierre Blondy, Sci. Technol. Adv. Mater. **11**, 065002 (2010).
[23] Y. W. Lee, B. J. Kim, J. W. Lim, S. J. Yun, Sungyoul Choi, B. G. Chae, G. Kim, and Hyun-Tak Kim, Appl. Phys. Lett. **92**, 162903 (2008).
[24] Joe Sakai, J. Appl. Phys. **103**, 103708 (2008).
[25] Hyun-Tak Kim, Bong-Jun Kim, Sungyoul Choi, Byung-Gyu Chae, Yong Wook Lee, Tom Driscoll, Mumtaz M. Qazilbash, and D. N. Basov, J. Appl. Phys. **107**, 023702 (2010).
[26] B. J. Kim, Giwan Seo, Y. W. Lee, Sungyoul Choi, and Hyun-Tak Kim, IEEE Electron Device Lett. **31**, 1314 (2010).
[27] Amos Sharoni, J. G. Ramírez, and I. K. Schuller, Phys. Rev. Lett. **101**, 026404 (2008).
[28] J. G. Ramírez, Amos Sharoni, Y. Dubi, M. E. Gomez, and I. K. Schuller, Phys. Rev. B **79**, 235110 (2009).
[29] Massimiliano Di Ventra, Yuriy V. Pershin, and Leon O. Chua, Proc. IEEE **97**, 1371 (2009).
[30] John Rozen, ReneÌ Lopez, Richard F. Haglund, and Leonard C. Feldman, Appl. Phys. Lett. **88**, 081902 (2006).
[31] Jun Dai, Xingzhi Wang, Ying Huang, and Xinjian Yi, Opt. Eng. (Bellingham, WA) **47**, 033801 (2008).
[32] Mei Pan, Hongmei Zhong, Shaowei Wang, Jie Liu, Zhifeng Li, Xiaoshuang Chen, and Wei Lu, J. Cryst. Growth **265**, 121 (2004).
[33] N. R. Mlyuka and R. T. Kivaisi, J. Mater. Sci. **41**, 5619 (2006).
[34] Jeehoon Kim, Changhyun Ko, Alex Frenzel, Shriram Ramanathan, and Jennifer E. Hoffman, Appl. Phys. Lett. **96**, 213106 (2010).
[35] Mumtaz M. Qazilbash, A. Tripathi, A. Schafgans, Bong-Jun Kim, Hyun-Tak Kim, Zhonghou Cai, M. Holt, J. Maser, F. Keilmann, O. Shpyrko, and D. Basov, Phys. Rev. B **83**, 165108 (2011).
[36] Alex. Frenzel, Mumtaz M. Qazilbash, M. Brehm, Byung-Gyu Chae, Bong-Jun Kim, Hyun-Tak Kim, A. Balatsky, F. Keilmann, and D. Basov, Phys. Rev. B **80**, 115115 (2009).
[37] N. A. Poklonski, A. A. Kocherzhenko, A. I. Benediktovitch, V. V. Mitsianok, and A. M. Zaitsev, Phys. Status Solidi B **243**, 1212 (2006).
[38] Dmitry Ruzmetov, Gokul Gopalakrishnan, Jiangdong Deng, V. Narayanamurti, and Shriram Ramanathan, J. Appl. Phys. **106**, 083702 (2009).
[39] G. Stefanovich, A. Pergament, and D. Stefanovich, J. Phys.: Condens. Matter **12**, 8837 (2000).
[40] Lionel Aigouy, Gilles Tessier, Michel Mortier, and Benot Charlot, Appl. Phys. Lett. **87**, 184105 (2005).
[41] J. S. Lee, M. Ortolani, U. Schade, Y. J. Chang, and T. W. Noh, Appl. Phys. Lett. **90**, 051907 (2007).
[42] J. S. Lee, M. Ortolani, U. Schade, Y. J. Chang, and T. W. Noh, Appl. Phys. Lett. **91**, 133509 (2007).
[43] Gokul Gopalakrishnan, D. Ruzmetov, and Shriram Ramanathan, J. Mater. Sci. **44**, 5345 (2009).
[44] Massimiliano Di Ventra, *Electrical Transport in Nanoscale Systems* (Cambridge University Press, Cambridge, UK, 2008).
[45] Feliks Chudnovskiy, Serge Luryi, and Boris Spivak, *Future Trends in Microelectronics: The Nano Millennium* (Wiley, Hoboken, NJ, 2002), pp. 148–155.
[46] Mumtaz M. Qazilbash, Z. Q. Li, V. Podzorov, M. Brehm, F. Keilmann, B. G. Chae, Hyun-Tak Kim, and D. N. Basov, Appl. Phys. Lett. **92**, 241906 (2008).
[47] Tai-Lung Wu, Luisa Whittaker, Sarbajit Banerjee, and G. Sambandamurthy, Phys. Rev. B **83**, 073101 (2011).
[48] Lev Vidmar, J. Bonča, Marcin Mierzejewski, Peter Prelovsek, and Stuart A. Trugman, Phys. Rev. B **83**, 134301 (2011).
[49] E. Arcangeletti, L. Baldassarre, D. Di Castro, S. Lupi, L. Malavasi, C. Marini, A. Perucchi, and P. Postorino, Phys. Rev. Lett. **98**, 196406 (2007).
[50] Jiang Wei, Zenghui Wang, Wei Chen, and D. H. Cobden, Nat. Nanotechnol. **4**, 420 (2009).
[51] Tao Yao, Xiaodong Zhang, Zhihu Sun, Shoujie Liu, Yuanyuan Huang, Yi Xie, Changzheng Wu, Xun Yuan, Wenqing Zhang, Ziyu Wu, Guoqiang Pan, Fengchun Hu, Lihui Wu, Qinghua Liu, and Shiqiang Wei, Phys. Rev. Lett. **105**, 226405 (2010).
[52] Bong-Jun Kim, Yong Wook Lee, Byung-Gyu Chae, Sun Jin Yun, Soo-Young Oh, Hyun-Tak Kim, and Yong-Sik Lim, Appl. Phys. Lett. **90**, 023515 (2007).
[53] Bong-Jun Kim, Yong Lee, Sungyeoul Choi, Jung-Wook Lim, Sun Yun, Hyun-Tak Kim, Tae-Ju Shin, and Hwa-Sick Yun, Phys. Rev. B **77**, 235401 (2008).
[54] Hyun-Tak Kim, Byung-Gyu Chae, Doo-Hyeb Youn, Gyungock Kim, Kwang-Yong Kang, Seung-Joon Lee, Kwan Kim, and Yong-Sik Lim, Appl. Phys. Lett. **86**, 242101 (2005).